Experimental Study of the Transition from Constrained to Unconstrained Growth during Directional Solidification.

Charles-André Gandin

▶ **To cite this version:**

HAL Id: hal-01564434
https://minesparis-psl.hal.science/hal-01564434

Submitted on 27 Jul 2017

Experimental Study of the Transition from Constrained to Unconstrained Growth during Directional Solidification

Ch.-A. GANDIN

Laboratoire de Science et Génie des Matériaux Métalliques, Ecole des Mines de Nancy, 54042 Nancy, France.
E-mail: gandin@mines.u-nancy.fr.

Temperature measurements are carried out in 99.99 wt% aluminium and aluminium–silicon alloys. The experimental apparatus was initially built for the study of microporosity formation in aluminium alloys.[1] The construction is designed to obtain upward directional solidification by limiting lateral heat flow during cooling and suppressing fluid flow induced by the pouring sequence. Cooling occurs from the top part of the ingot, leading to the formation of a surface dendrite layer. In the 99.99 wt% aluminium, very few equiaxed grains sink down from the surface dendrite layer into the liquid. The density of the equiaxed dendritic grains is too low to block the columnar cellular front. Cooling curves show that, once superheat disappears (*i.e.*, when no substantial thermal gradient remains in the liquid), the liquid is kept at an almost constant temperature during the growth of the columnar front and a small negative thermal gradient forms in the liquid ahead of the growing columnar front. It is concluded that the liquid is reheated by the growing columnar front. In the case of the aluminium–silicon alloys, a columnar-to-equiaxed transition (CET) is observed at almost two-thirds of the ingot length. The columnar length is found to increase slightly with decreasing the solute content. Recalescence is measured in a fully equiaxed region, while cooling rate, recorded by the thermocouple located just above the CET, remains negative.

KEY WORDS: solidification; columnar grain structures; constrained and unconstrained growth.

1. Introduction

The columnar-to-equiaxed transition (CET) is a common grain structure feature of cast metals.[2,3] It corresponds to a transition in the morphology of the grains formed during solidification of the melt. Grains in columnar zones of cast metals appear elongated in metallographic sections made parallel to the heat flow direction. They are characterised by a large shape factor. On the contrary, grains in equiaxed zones are found rather round in shape. They form in a uniform temperature environment, *i.e.* in a melt which cools in almost all directions without preferred heat flow direction. Both types of structures are made visible in the ingots shown in **Fig. 1**, with a CET occurring at about two-thirds of the ingots length in the aluminium–silicon alloys.

Another way to differentiate between columnar and equiaxed grains, which is commonly mentioned in the literature, is by considering the local growth conditions in which the dendrites develop.[4] Columnar grains are formed when the growth directions of the dendrite trunks are close to the direction of the thermal gradient in the liquid. This situation is referred to as growth in a positive thermal gradient. In vertical Bridgman-like cooling conditions (*i.e.*, when both the thermal gradient and the velocity of the isotherms are imposed), a fictitious macroscopic interface can be defined by a horizontal surface on which the dendrite tips lie. Above this surface, the metal is fully liquid, whereas below it is mushy (*i.e.*, partially solidified and

made of solid dendrites). In stationary growth conditions, the velocity of this interface is simply that given by the isotherms. It corresponds to the velocity at which the dendrite tips are growing. Direct measurements of the temperature of the dendrite tips show that the interface grows with a certain degree of undercooling.[5] Dendrite tip growth kinetics models have been developed in order to determine this undercooling as a function of the local cooling conditions.[6–8] These assume that the dendrites grow in a mean positive temperature gradient, thereby not distinguishing between the values of the thermal gradients in the liquid and in the mush (*i.e.* ahead and below the growing dendritic interface). The result for the dendritic growth regime can usually be approximated by a simple velocity versus undercooling relationship.

Equiaxed grains are formed by the free growth of dendrites into an undercooled melt.[4] This means that the growth direction of the dendrites is opposite to the direction of the thermal gradient in the liquid, while the solid is maintained at an almost constant temperature. This situation is referred to as growth in a negative thermal gradient. The overall shape of a fictitious macroscopic interface, which would enclose the dendrite tips of an equiaxed grain, is not obvious to predict. Authors usually assume simple and unchanged morphologies of the growing shape (*i.e.*, sphere, octahedron or stars with six orthotropic branches representing the $\langle 100 \rangle$ preferred dendrite growth directions) which enclose the mush and is fully surrounded by liq-
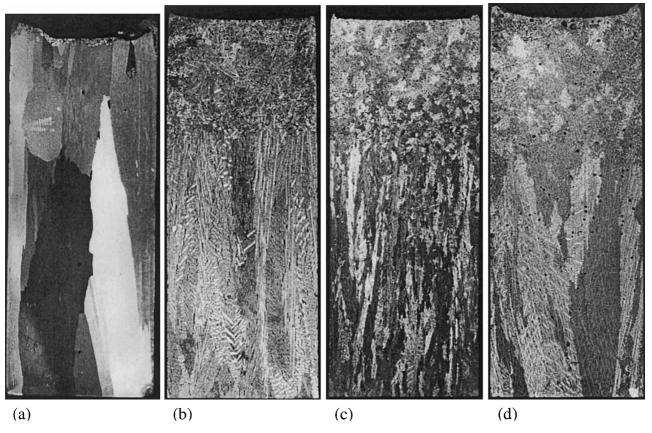
Fig. 1. Experimental grain structures observed in longitudinal cross sections of cylindrical aluminium–silicon ingots obtained by directional solidification over a copper chill. Lengths measured at the vertical centrelines of the cross sections: (a) $0.164 \pm 0.5 \cdot 10^{-3}$ m and (b)–(d) $0.170 \pm 0.5 \cdot 10^{-3}$ m. Diameters: 0.070 m (measured at the root of the cylinders in contact with the chill) and composition: (a) 99.99 wt% Al (b) Al–3wt%Si, (c) Al–7wt%Si and (d) Al–11wt%Si. Casting temperature: (a) 759°C, (b) 763°C, (c) 746°C and (d) 768°C. Height of the CET measured from the bottom of the ingots by considering the highest directionally grown dendrites found in the columnar zone: (b) 0.120 ± 0.001 m, (c) 0.118 ± 0.001 m and (d) 0.109 ± 0.001 m. Cross sections were not precisely performed at the centre of the cylinders, which explains why the picture ratios height/width do not exactly correspond to the real ratios of length/diameter.

uid.[9–11] These morphologies are based on experimental observation[12] and can eventually change with the local cooling conditions.[11,13] The kinetics models dedicated to the free growth in the undercooled melt consider dendrites growing in an infinite bath with a fixed undercooling, which is kept unchanged during growth.[14,15] They are usually applied assuming no thermal gradient in the solid.

The differences in the temperature profiles assumed for the modelling of columnar and equiaxed growth have been summarised in the literature.[4,16] Columnar and equiaxed growth regimes are referred to respectively as constrained and unconstrained. Indeed, constrained growth is used to characterise an interface growing in a direction opposite to that of heat flow (*i.e.*, growth in a positive thermal gradient in the liquid); while unconstrained growth refers to the opposite situation (*i.e.*, growth in a negative thermal gradient in the liquid). As a result, constrained growth leads to the growth of a thermally stable interface, while unconstrained growth does not.[4] But this stability analysis is obtained by considering the growth of a flat solid-liquid interface. In conventional casting of alloys, the interface is rather cellular or dendritic due to the destabilisation induced by solute segregation. Definitions of constrained and unconstrained growth can still be used with respect to the thermal gradient in the liquid. Constrained growth would then occur if a positive thermal gradient existed ahead of the fictitious macroscopic interface defined by joining the dendrite tips of the columnar front, while unconstrained growth would refer to the opposite situation.

Temperature measurements during directional solidification of dendritic alloys have already been presented.[17–19] Only the recent measurements by Fernihough *et al.*[19] were shown to offer sufficient precision for a fine analysis of the cooling conditions when the columnar front reaches the CET position. However, these authors used sophisticated nickel-base superalloys for which the relationship between the dendrite tip velocity and the undercooling is not accurately known. Only an extension to multicomponent systems of a dendrite tip kinetics model designed for binary alloys was used,[20] which was not validated by temperature measurements of the dendrite tips for sophisticated nickel base superalloys. In addition, their experimental apparatus did not impose the velocity of the columnar front which evolved with time. Consequently, their analyses was made difficult without the use of a modelling approach resolving both the velocity and the thermal gradient on each side of the macroscopic interface at the CET position.[21]

The purpose of the present contribution is to study experimentally, the local cooling conditions in the vicinity of the columnar interface up to the position of the CET. Measure-
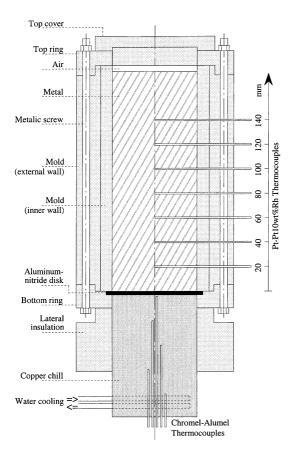
Fig. 2. Schematics of the apparatus used for the unidirectional solidification experiments.

ments in directionally solidified 99.99 wt% aluminium and aluminium–silicon alloys were carried out and are analysed in this article. These measurements are used elsewhere for the validation of a numerical one-dimensional solidification model.[22]

2. Experimental

An experimental apparatus for the study of porosity formation during solidification of aluminium alloys was designed by Ampuero et al.[1] It was later used by Gandin and Rappaz[13] and Rousset et al.[23] to study the columnar-to-equiaxed transition and macrosegregation, respectively. A detailed description is given hereafter with a schematic diagram presented in **Fig. 2**.

A cylindrical mould was made from several components of a highly insulating ceramic material, PYROTEK N-101[*1] These components were the inner and outer cylindrical mould walls, bottom and top rings, as well as a top cover. The cylindrical walls and rings were held together using metallic screws. Once assembled, the inner dimensions of the mould were 70 mm in diameter and 185 mm height. The construction of the assembly was designed to minimise lateral heat losses during cooling of the metal through the cylindrical mould walls, as well as from the

metal-air free surface. The total thickness of the mould walls was 30 mm and the cover was exactly fit into the top ring. This cover was kept in position during the entire time of the experiment, except for the filling of the mould with the liquid metal. The bottom part of the mould was closed with a thin aluminium–nitride disc[*2] and alumina powder was spray coated on its top surface. The thin disc was fitted into the bottom ring and held in place by the inner ceramic walls.

Special care was taken to prevent leakage of liquid metal. This is a crucial point since the metal was maintained in the liquid state for at least one hour in the mould prior to the start of the solidification experiment. For that purpose, seals were cut out of a thin blanket made of fibres[*3] and positioned at all critical interfaces between the various parts of the mould. In spite of the fact that two layers of ceramic were used for the construction of the mould (inner and outer mould walls), the external radius of the inner layer equalled the internal radius of the outer layer so that they fitted perfectly into each other.

Seven Pt–Pt10wt%Rh thermocouples were positioned at 20 mm intervals on the centreline of the cylinder from the inner bottom surface of the mould (i.e., from the top surface of the aluminium–nitride disk). These thermocouples were made of 0.2 mm wires enclosed in 1 mm alumina tubes. They entered into the mould by small horizontal holes prepared into the cylindrical ceramic walls. Their junction were directly in contact with the liquid metal so as to provide a very fast response time. Thermocouple voltages were recorded at least every second using a data acquisition system controlled by a computer.

The experimental procedure was as follows. At first, both the mould and the liquid metal were kept in two separate furnaces at the desired casting temperature for several hours. With the mould still in the furnace, the metal was poured and the system was kept in the furnace for at least one hour to reach a homogenised temperature throughout the liquid metal. Once a uniform temperature was reached (i.e. when less than 1°C of difference was registered between the seven thermocouples located in the melt), the furnace was lowered away from the mould. This operation was made without moving the mould in order to avoid mechanically inducing movement in the liquid. A water-cooled copper chill was then immediately raised to touch the bottom of the aluminium–nitride disk, thus starting the cooling and upward directional solidification of the metal. Data acquisition was started approximately two minutes prior to removing the furnace in order to record the entire solidification sequence. The measurements showed that the initial temperatures ranged from 746°C to 768°C in the four experiments presented in Fig. 1.

Two goals were to be achieved with this experimental set-up: first, convection associated with the pouring of the liquid into the mould must be eliminated, and second, unidirectional heat flow must be achieved and maintained. Although no direct observation can be made of the fluid

---

*1 PYROTEK-N 101 is a trademark of PYROTEK ENGINEERING MATERIALS, LTD, Milton Keynes, United Kingdom. Its thermal conductivity is in the order of 0.1 W m^{-1} K^{-1}.

*2 Aluminum–nitride is known for its fairly high thermal conductivity, i.e., of the order of 150 W m^{-1} K^{-1}.

*3 The insulation blanket used is made of alumina and silica fibers by INSULTECH A.G., Wangen b. Olten, Switzerland. Its thermal conductivity at 600°C is in the order of 0.1 W m^{-1} K^{-1}.
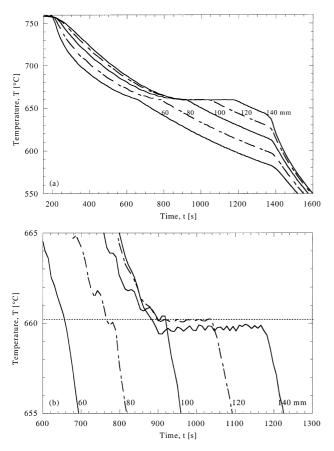
Fig. 3. Recorded cooling curves at different heights from the bottom of the ingot in the 99.99 wt% Al ingot shown in Fig. 1(a). Figure 3(b) is a magnification of Fig. 3(a) made in a narrow range of temperature surrounding the melting temperature (horizontal dotted line at 660.2°C).
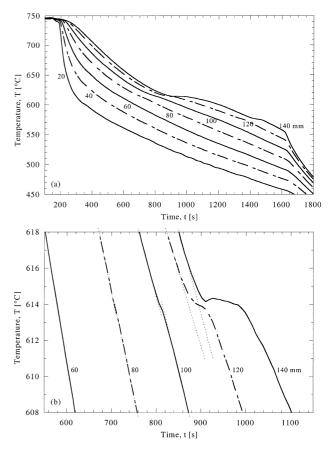
Fig. 4. Same as Fig. 3 for the Al–7wt%Si alloy. The magnification in Fig. 4(b) is made in a narrow temperature region below the liquidus temperature (618°C), while the range of the time scale covers the period during which the transition from a columnar to a fully equiaxed grain structure occurs. Fine dotted lines are superimposed on the cooling curves to visualise the cooling rates and slope changes due to the growth of the columnar front.

flow in the mould, the first point was obviously achieved due to the experimental procedure. The second point was confirmed by measuring the lateral temperature gradient during solidification in one of the experiments carried out by Ampuero.[24] An additional thermocouple was introduced in the metal, close to the mould wall at the same height as one of those shown in Fig. 2. A temperature difference of the order of 1°C was recorded between these two thermocouples during the entire solidification experiment. Not only was this a proof for the unidirectional heat flow, but also this shows that the driving force for natural thermal convection was negligible.

Metals cast were 99.99 wt% aluminium and aluminium–silicon alloys with 3, 7 and 11 wt% silicon. No addition of inoculation particles (such as TiB_2) was carried out to the liquid melts. Buoyancy forces induced by segregation in the liquid state must also be considered. These forces, when sufficiently developed, induce macrosegregation and eventually lead to freckling.[23,25–27] As the density of molten aluminium–silicon alloys appears to increase with silicon content,[28] buoyancy forces induced by segregation will not appear and macrosegregation is therefore not taken into account in this work.

Longitudinal sections of the cylindrical aluminium and aluminium–silicon ingots were mechanically polished using abrasive papers with successively finer SiC particles, and subsequently etched with an acid solution (20 m*l* HCl, 20 m*l* HNO_3, 5 m*l* HF for 25 m*l* H_2O).

3. Cooling Curves Analysis

Cooling curves recorded every 20 mm from the bottom of the ingot are shown in **Figs. 3** and **4** for the 99.99 wt% Al and the Al–7wt%Si alloy, respectively. The trends observed for the Al–7wt%Si alloy are similar for the Al–3wt%Si and Al–11wt%Si alloys. Consequently, only a detailed analysis for the Al–7wt%Si alloy is carried out hereafter.

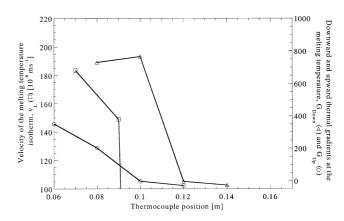### 3.1. 99.99 wt% Aluminium Ingot

Thermocouples located at positions 20 and 40 mm did not function correctly in the solidification experiment carried out with the 99.99 wt% Al. Consequently, only records obtained for thermocouples located from 60 to 140 mm are plotted in Fig. 3. As can be seen, thermocouples located at 120 and 140 mm show a temperature plateau. These plateau end when the thermocouples are reached by the columnar front and heat is conducted through the solid. The plateau temperature of the thermocouple located at 120 mm is clearly very close to the melting temperature of pure aluminium reported in the literature[29] (*i.e.*, 660.2°C). The undercooling of the columnar front is estimated to be less than one degree for the last thermocouple.
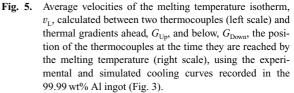
The cooling curves also show that the three last thermocouples have intersecting temperature evolutions occurring

above the melting temperature of pure aluminium (*i.e.*, in the liquid state). This inversion of the temperature profile is consistent with the increase of the cooling rate measured in the liquid from 100 to 140 mm (compare the slopes of the cooling curves above 660.2°C for the last three thermocouples). This can only be explained by cooling from the top surface of the ingot. This means that, in spite of the hot top cover (Fig. 2), heat loss takes place through the metal–air interface. A downward thermal gradient thus forms after 850 s between the three last thermocouples as a result of the cooling from the top surface. Proof of a downward thermal gradient is also made apparent by a simple reading of the temperatures recorded by the two last thermocouples between 900 and 1050 s.

A slight increase in the liquid temperature is also observed on the plateau of the last thermocouple. It shows that the growth of the directionally solidified structure toward the highest thermocouple is accompanied by an increase of the liquid temperature. Such an observation reveals the presence of a small negative thermal gradient (less than 1°C over a 20 mm distance) with respect to the columnar growth direction in the present experiment, which is indeed consistent with the reported downward thermal gradient in the top part of the liquid. This observation can be used as a proof that heat released by the directionally growing interface reheats the liquid when no substantial thermal gradient remains in the liquid. This observation of liquid reheating obviously stops at the time when the solid columnar front reaches the thermocouple position.

A surface dendrite layer is observed at the top of Fig. 1(a). The formation of such a structure is clearly due to the cooling of the top part of the ingot below the melting temperature of the 99.99 wt% Al from the metal–air interface. However, the temperature profiles required in the surface dendrite layer and in the liquid for the formation of these dendrites is that of free growth: an almost zero thermal gradient in the solid together with a negative thermal gradient in the liquid with respect to the growth direction of the dendrites. This situation would correspond to an upward vertical thermal gradient in the liquid for a downward growth direction of the dendrites nucleated at the metal–air interface. Despite the heat loss through the metal–air interface, the dendrite layer would thus be maintained at a higher temperature than that of the liquid located underneath. This conjecture, however, cannot be directly confirmed using the recorded cooling curves. It is possible that heat released during the growth of the dendrite layer partly compensates for the heat loss through the top surface of the ingot. It thus forms a barrier which, once formed, probably contributes to prevent a continuous cooling of the top liquid region.

From these information, reconstruction of a temperature profile from the bottom to the top of the ingot at time 950 s would thus show (i) a solid region in which the temperature increases from the bottom of the ingot to the cellular columnar interface located between 100 and 120 mm, (ii) an undercooled liquid region with a small decrease of the temperature when increasing the distance from the columnar interface (*i.e.*, a negative thermal gradient with respect to the growth direction of the columnar interface), (iii) a surface layer made of dendrites with a temperature below the melting temperature of pure aluminium.
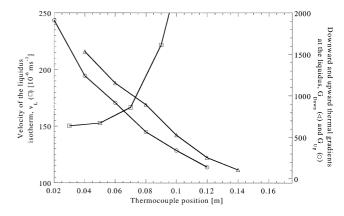

Fig. 5. Average velocities of the melting temperature isotherm, v_L, calculated between two thermocouples (left scale) and thermal gradients ahead, G_{Up}, and below, G_{Down}, the position of the thermocouples at the time they are reached by the melting temperature (right scale), using the experimental and simulated cooling curves recorded in the 99.99 wt% Al ingot (Fig. 3).

Fig. 6. Same as Fig. 5 for the cooling curves recorded in the Al–7wt%Si ingot (Fig. 4) and using the liquidus temperature isotherm of the alloy.

3.2. Aluminium–Silicon Ingots

As in the case of Fig. 3, Fig. 4 is split into two graphs, one presenting the cooling curves in the overall solidification interval, the other magnifying a narrow temperature region below the liquidus temperature. In Fig. 4(b), the last cooling curves are not found to intersect as in the case of Fig. 3(b). However, the heat loss through the top surface is confirmed by the slightly higher cooling rate recorded on thermocouple located at 140 mm compared to that located at 120 mm (the negative value of the curve slope at 140 mm is smaller than that at 120 mm). An inversion of the temperature profile, similar to that reported for the 99.99 wt% Al, is thus expected to occur above 140 mm.

Magnification of the cooling curves (Fig. 4(b)) clearly reveals slope changes below the liquidus isotherm (618°C) associated with the formation of the dendritic grain structure. The effect of the columnar dendrites passing the thermocouples becomes visible when the cooling rate decreases, *i.e.*, for thermocouples located at 80 and 100 mm. The slope change is observed for an undercooling higher than 4°C. The last two thermocouples are located in the equiaxed zone. A recalescence is usually expected due to the growth of equiaxed crystals. However, recalescence is only measured with the highest thermocouple. The reason

for the absence of a recalescence measured on thermocouple 120 mm is that the heat extracted through the solid and the mushy zone is larger than the heat released during equiaxed growth. This has already been shown by coupling nucleation and growth mechanisms of dendritic grain structures with a finite element prediction of the heat flow.[13]

4. Equilibrium Isotherm Velocity and Thermal Gradients

Figures 5 and **6** present respectively the average velocities of the equilibrium isotherm for the 99.99 wt% Al and the Al–7wt%Si alloy. The procedure to produce these curves was as follows: the time, t_I, at which a thermocouple located at position x_I ($x_I = [20, 40, \ldots, 140 \text{ mm}]$ for $I = [1, 2, \ldots, 7]$) attains the equilibrium temperature, T_L, is noted within the recorded temperature evolutions, T_I (*i.e.*, t_I such that $T_I(t_I) = T_L$). The distance between two consecutive thermocouple positions, $x_{I+1} - x_I$, divided by the time difference found between these positions, $t_{I+1} - t_I$, gives the average velocity required for the equilibrium isotherm to travel from one thermocouple position to the other: $\bar{v}_{L,I:I+1} = (x_{I+1} - x_I)/(t_{I+1} - t_I)$. The average velocity is then drawn at the middle position between the two adjacent thermocouples, $(x_I + x_{I+1})/2$.

Also shown in Figs. 5 and 6 are the downward, $G_{\text{Down},I}$, and upward, $G_{\text{Up},I}$, thermal gradients at time t_I when the thermocouple located at position x_I attains the equilibrium temperature. They are evaluated by considering the temperature of the downward and upward closest thermocouples: $G_{\text{Down},I} = (T_I(t_I) - T_{I-1}(t_I))/(x_I - x_{I-1})$ and $G_{\text{Up},I} = (T_{I+1}(t_I) - T_I(t_I))/(x_{I+1} - x_I)$, respectively.

Figure 5 shows that negative values of the average velocity of the equilibrium isotherm are calculated. This is due to the intersection of the cooling curves above the melting temperature at positions higher than 100 mm (Fig. 3). In Fig. 6, the average velocity is observed to rise abruptly above 70 mm to reach unreasonable values in the upper part of the ingot. These two effects are due to the cooling from the top part of the ingot associated with the decrease of the thermal gradient in the liquid. Therefore, the cooling curves can not be used directly to determine the growth rate of the microstructure.

In Fig. 5, an abrupt decrease of the downward thermal gradient is observed, which again is due to the intersection of the cooling curves. The two last thermocouples attain the equilibrium temperature at around 900 s. But the growth front passes the 120 and 140 mm thermocouples at around 1050 and 1150 s, respectively. Thus, G_{Down} and G_{Up} do not correspond to the thermal gradient below and ahead the growing interface (*i.e.*, in the liquid and in the mush, respectively). Consequently, erroneous interpretation are expected if the temperature of the equilibrium isotherm is assimilated to that of the growing interface, thus badly estimating the position of the columnar front. In fact, a correct interpretation of the cooling curves can only be made by tracking the front position and temperature with time. This is demonstrated in the modelling approach developed in.[22]

5. Grain Structures Analysis

Four regions of grain structures are often distinguished in casting[2,3]: 1 - the outer equiaxed zone (or skin zone) located in the vicinity of the mould walls, 2 - the columnar zone composed of elongated grains, 3 - the inner equiaxed zone observed in the central part of the casting and 4 - the surface dendrite layer formed on a metal–air interface.[30] With the directional solidification apparatus schematised in Fig. 2, these four zones are expected to be found 1 - at the bottom of the ingot above the aluminium–nitride disk, 2 - above the outer equiaxed zone, 3 - in the top part of the cylindrical mould and 4 - just below the metal–air interface. In Fig. 1(a), mainly columnar grains are seen with no internal dendritic morphology, together with a few equiaxed grains, partly dendritic, in the upper part of the casting. A thin surface dendrite layer is also present at the top surface of the casting. Figures 1(b)–1(d) show that approximately two-thirds of the aluminium–silicon ingots are composed of a columnar dendritic grain structure, above which is located a region of equiaxed dendritic grains. No outer equiaxed region is found in Figs. 1(a)–1(d). Also, if a surface dendrite layer forms at the top of the aluminium–silicon ingots, it is not clearly evident in Figs. 1(b)–1(d).

5.1. 99.99 wt% Aluminium Ingot

In Fig. 1(a), the elongation of the columnar grains and the ingot heights are of the same order of magnitude. Some columnar grains have even grown without interruption from the bottom to the top of the ingot. Perturbation analysis predict no destabilisation of a pure metal interface grown in a positive thermal gradient (*i.e.*, when the growth direction is opposite to the heat flow direction).[4] In practice, the directionally grown primary aluminium interface is most probably cellular due to its destabilisation by segregated impurities. Indeed, a fine pattern appears within each grain which can be seen as the result of cellular growth (not visible with the low magnification used in Fig. 1(a). However, segregation is too low to lead to the precipitation of second phases in between the cells of the primary grown structure, as is usually the case for interdendritic solidification of alloys.

In the longitudinal cross section shown in Fig. 1(a), four equiaxed dendritic grains can be seen, in addition to those connected to the top surface of the ingot. These four grains are composed of a dendritic core surrounded by a cellular halo, both having the same crystallographic orientation as was verified using a Laue X-ray diffraction apparatus. The three small equiaxed dendrites located in a 20 mm region below the top surface undoubtedly correspond to "comet" grains as identified by Southin.[30] That is, they come from dendrites which were detached from the surface dendrite layer and then sank down into the liquid. Once reaching the directionally growing cellular structure, they develop a directional cellular structure (*i.e.*, the halo) similar to that of the columnar grains. As a consequence, these comet grains are made of a dendritic head and a cellular tail. This point is important since it can be used as a proof of a change occurring in the growth regime. In fact, formation of dendrites in pure metals is only possible in a free growth or unconstrained regime (*i.e.*, in an undercooled melt, heat being extracted through the liquid phase and growth of the den-

drite tips proceeding in the presence of a negative thermal gradient in the liquid while almost no thermal gradient exists in the solid). If cellular growth observed in the columnar zone is the result of constrained growth, a comet grain would thus be explained by a transition from an unconstrained to a constrained growth regime occurring once the grain has sunk onto the columnar interface and heat can be preferentially extracted through the columnar zone.

The larger dendritic grain found at a lower position below the top surface (its lowest position in Fig. 1(a) is at 106 mm from the bottom of the ingot) presents a more isotropic cellular halo. Therefore, it does not strictly look like a comet grain. In order to verify whether or not this grain could originate from the surface dendrite layer, one needs to further analyse the cooling situation that existed during the solidification experiment.

Figure 3(b) shows that the three last thermocouples fall below the melting temperature (660.2°C) around 900 s within a narrow time interval. This means that the zone of undercooled liquid is almost 70 mm long at that time, thus largely enclosing the zone where the large equiaxed grain is found. It can thus be concluded that if a dendrite is nucleated at the metal–air interface shortly after the top surface becomes undercooled (*i.e.*, before 900 s), it detaches and grows substantially while it sinks, it could finish as the origin of the large dendritic grain seen 40 mm below the top surface. As soon as the large equiaxed dendrite touches the directionally grown cellular front, heat is preferentially conducted through the columnar zone, thus forming the cellular region surrounding the dendrite (similar unconstrained to constrained growth transition as for the three small comet grains).

5.2. Aluminium–Silicon Ingots

All aluminium–silicon ingots shown in Figs. 1(b)–1(d) exhibit a columnar-to-equiaxed transition occurring at approximately two-thirds of the ingot length. The CET positions from the bottom of the ingot are reported in the figure caption. The columnar length is found to increase slightly when the solute content is decreased. However, differences are observed on the morphological transition: transition is sharp in the case of Al–3wt%Si and Al–11wt%Si, and progressive in the Al–7wt%Si. Both the columnar and equiaxed zones of the Al–3wt%Si and Al–11wt%Si ingots are characterised by low grain densities compared with the Al–7wt%Si ingot. The top part of the columnar zone is made of elongated dendrites with a small transverse size, mixed with equiaxed grains for the Al–7wt%Si alloy. A second experiment with the same Al–7wt%Si alloy was carried out and showed the same grain structure evolution.[13]

As pointed out earlier, a surface dendrite layer can not be clearly distinguished at the top of the aluminium–silicon ingots. This is partly due to the fact that, if an unconstrained to constrained growth occurs during the formation of the equiaxed dendritic grains, it is not accompanied by the same dendritic to cellular morphological transition as in the case of the 99.99 wt% Al. Growth kinetics of the dendrites in the dilute aluminium–silicon alloys used is mainly driven by diffusion of solute elements segregated in the liquid. Consequently, cellular growth is not expected to take place

in the thermal cooling conditions of the experiments. Southin[30] has shown that the dendritic structure developed in the fourth zone differs sufficiently from that forming later when grains have detached from the top surface. However, his studies have also shown that this transition is only clearly revealed for low dilute aluminium–copper alloys, but hardly seen when increasing the solute content. Since the slope of the cooling curves (see Fig. 4 for the Al–7wt%Si alloy) show that cooling from the metal–air interface occurs, surface dendrites are definitively suspected to form. It is thus concluded that silicon content is too high to distinguish two growth sequences in the dendritic microstructures of the equiaxed grains.

The detachment of dendrite fragments from the top metal–air interface of the 99.99 wt% Al ingot is too infrequent to block the growth of the columnar grains. This is due to the low heat loss through the metal–air interface which does not permit sufficient cooling of the top surface region. Thus, limited nucleation and growth rates of surface dendrites are reached, without promoting the formation of a large population of comet grains.[30,31] Equiaxed grain density in the aluminium–silicon ingots is much higher than for the 99.99 wt% Al ingot and a CET is found at two-thirds of the ingot lengths. It may be argued that the fourth zone develops sufficiently in dendritic alloys to explain the origin of the entire equiaxed zones in Figs. 1(b)–1(d).[31] However, heterogeneous nucleation in the bulk liquid can not be totally ruled out.[32] This mechanism was modelled by Gandin and Rappaz[13] for predicting the CET in an Al–7wt%Si alloy using a distribution of nucleation sites. It should be noted that no addition of inoculation particles was made to the alloys. Thus, without a direct in-situ observation of the solidification sequence, doubts subsist on the origin of the equiaxed grain structure.

6. Discussion

6.1. 99.99 wt% Aluminium Ingot

As previously explained in the introduction, constrained and unconstrained growth are characterised respectively by positive and negative thermal gradients in the liquid ahead of the growing interface. This definition is based on the study of the thermal stability of a planar interface with respect to a small perturbation. The observation of a negative thermal gradient in the liquid ahead of the columnar interface might thus be interpreted as a transition from a constrained to an unconstrained growth regime, the opposite to what was found for the comet grains. Since the last thermocouple is clearly located in a cellular region, a destabilisation of the cellular interface induced by the local thermal conditions in the liquid might thus be expected. This would lead to a cellular to dendritic transition. Instead, cellular growth is observed. The grain located at 40 mm from the top surface even shows a stabilisation of its initially dendritic morphology once it falls down the columnar front.

In fact, a major difference is observed with the equiaxed dendritic growth regime occurring in a uniform undercooled zone and characterised by a negative thermal gradient ahead of the dendritic interface: a large positive thermal gradient exists in the solid region consisting of columnar

grains. The destabilisation of an interface during unconstrained growth is due to the release of the heat associated with the phase change which must be conducted through the liquid. Since most of the heat released can still be conducted through the columnar solid in the present experiment, cellular growth is observed in spite of the unstable nature of the thermal conditions measured in the liquid. It should also be pointed out that the negative thermal gradient is very small (less than 1°C over a 20 mm distance), leading to a small driving force for destabilisation. Thus, the definitions of constrained and unconstrained growth regimes should account for both the thermal gradient in the liquid and in the solid, as is usually the case in a stability analysis performed for a flat interface.[33]

6.2. Aluminium–Silicon Ingots

The columnar length is found to increase with decreasing the solute content. This result agrees well with Mahapatra and Weinberg[17] experiments in tin-lead alloys. These authors have also proposed that, for a given alloy composition, CET would occur at a fixed thermal gradient taken in the liquid at the liquidus temperature. Ziv and Weinberg later supported this finding in aluminium–copper alloys.[18] However, the estimation of the value of the thermal gradient was made using either the cooling curves[18] or a numerical model which did not account for columnar dendrite tip undercooling.[17] The accuracy of the values proposed for the thermal gradient at which CET would occur for a given alloy, or the soundness of a CET criterion based on reaching a given value of the thermal gradient in the liquid,[34] are open to discussion. Small values of the estimated thermal gradient in the liquid are proposed: 60°C/m in Al–3wt%Cu and 100°C/m in Sn–5wt%Pb. These findings agree well with the excellent measurements carried out in nickel base superalloys by Fernihough et al.[19] who also found very flat temperature profiles in the liquid ahead of the growing interface at the time estimated for the CET. Obviously, the experimental results presented in this contribution for the Al–7wt%Si alloy are very similar to those reported previously. As may be seen in Fig. 6, the upward temperature gradient close to the CET position (thermocouple located at 120 mm) at the liquidus temperature is equal to 140 K/m in the Al–7wt%Si alloy. It should yet be recalled that this value is only an estimation since columnar dendrites are growing several degrees below the liquidus isotherm and the CET occurs below to the thermocouple position.

Pollock and Murphy[27] have also carried out observations in unidirectionally solidified nickel base superalloys. They measured the breakdown of a single crystal into columnar and latter equiaxed grains. They observed that the breakdown of the single crystal occurred when the primary dendrite arm spacing exceeded a critical value, corresponding to a morphological transition in the dendritic array. These authors also identified freckles formed within the columnar grains, which is a proof that thermosolutal convection took place in their experiments. Such convection induced by segregation does not occur in the aluminium–silicon experiments presented above. And a clear morphological transition is not obvious to observe since the columnar zone is not made of a single crystal. However, since interaction of the growing columnar front with the local temperature field

is attested by liquid reheating in the 99.99 wt% Al, a similar effect for the Al–Si dendritic alloys when reaching a sufficiently small thermal gradient in the liquid may occur. Dendrite arm detachment and fragmentation might occur due to lateral diffusion of heat around the dendrite trunks. This could then result in similar morphological transition in the dendritic array as observed by Pollock and Murphy.[27]

7. Conclusion

Unidirectional solidification experiments have been carried out in 99.99 wt% Al and aluminium–silicon alloys. Simultaneous analyses of the recorded temperature history and of the grain structures lead to the following conclusions:

(1) Cooling from the top metal–air interface takes place with the unidirectional solidification apparatus designed by Ampuero et al.[1] This leads to the formation of a surface dendrite layer at the top of the 99.99 wt% Al ingot. A surface dendrite layer cannot be distinguished from the equiaxed grain structures in the aluminium–silicon ingots. It is however suspected to form and to be one of the sources of equiaxed grains, as was shown in previous experimental studies.[30,31]

(2) Once superheat vanishes in the 99.99 wt% Al ingot, a large zone of liquid kept at an almost constant temperature form ahead of the columnar zone. In front of the growing columnar interface, a small negative thermal gradient appears, of magnitude less than 1°C over a 20 mm distance. This is due to the latent heat released at the interface which is partly conducted in the liquid. This observation shows that the growing columnar structure can strongly influence the temperature gradient in which it develops. This phenomenon is not directly measured for the aluminium–silicon alloys. Instead, an equiaxed grain structure forms. If latent heat is also partly released in the liquid aluminium–silicon alloys when the thermal gradient decreases significantly, it is expected to have an influence on the growing dendritic interface. This should be studied in more details to determine if dendrite arm remelting and fragmentation could occur within the columnar dendritic array, leading to the breakdown of the columnar front as observed by Pollock and Murphy.[27]

(3) The stability analysis of a planar interface, initially developed by Mullins and Sekerka,[33] considers the thermal gradients in the solid and in the liquid. It is usually applied to growth kinetics model developed for columnar dendrites assuming a mean thermal gradient across the interface.[7] This approximation is no longer correct for the 99.99 wt% Al experiment since a positive thermal gradient is maintained in the solid and a small negative thermal gradient develops in the liquid.

(4) The columnar length is found to increase with decreasing solute content. This observation, as well as the order of magnitude of the estimated thermal gradient in the liquid when the CET occurs (i.e., 140°C/m in the Al–7wt%Si), agrees with other experimental results reported in the literature.[17–19,27]

(5) The growth rate of the columnar front, as well as the thermal gradient in the liquid and in the mush, cannot be directly deduced from the recorded cooling curves. They

require a more precise analysis, in which the undercooling of the growing front is taken into account. This is the purpose of the modelling work presented elsewhere.[22]

(6) The microstructural change in the comet grains consisting of a dendritic head and a cellular tail are attributed to an unconstrained to constrained transition in the growth regime.

(7) The sharpness of the CET is observed to vary in the aluminium–silicon ingots as a function of the composition. This variation is not clearly understood.

REFERENCES

1) J. Ampuero, A. F. A. Hoadley and M. Rappaz: Modeling of Casting, Welding and Advanced Solidification Processes, Ed by M. Rappaz, M. Özgü and K. W. Mahin, TMS, Warrendale, PA, (1991), 449.
2) B. Chalmers: Principles of solidification, John Wiley & Sons, New York, (1964).
3) M. C. Flemings: Solidification Processing, Mc Graw-Hill, New York, USA (1974).
4) W. Kurz and D. J. Fisher: Fundamentals of Solidification, Trans. Tech. Pub., Aedermannsdorf, Switzerland, (1989).
5) M. H. Burden and J. D. Hunt: *J. Cryst. Growth*, **22** (1974), 99.
6) M. H. Burden and J. D. Hunt: *J. Cryst. Growth*, **22** (1974), 109.
7) W. Kurz, B. Giovanola and R. Trivedi: *Acta Metall.*, **34** (1986), 823.
8) J. D. Hunt: *Acta Metall. Mater.*, **38** (1990), 411.
9) M. Rappaz and Ph. Thévoz: *Acta Metall.*, **35** (1987), 1487.
10) C. Y. Wang and C. Beckermann: *Metall. Trans.*, **24A** (1993), 2787.
11) Ch.-A. Gandin and M. Rappaz: *Acta Metall. Mater.*, **45** (1997), 2187.
12) D. E. Ovsienko, G. A. Alfintsev and V. V. Maslov: *J. Cryst. Growth*, **26** (1974), 233.
13) Ch.-A. Gandin and M. Rappaz: *Acta Metall.*, **42** (1994), 2233.
14) J. Lipton, M. E. Glicksman and W. Kurz: *Metal. Trans.*, **18A** (1987), 341.
15) J. Lipton, W. Kurz and R. Trivedi: *Acta Metall.*, **35** (1987), 957.
16) R. Trivedi and W. Kurz: *Int. Mater. Rev.*, **39** (1994), 49.
17) R. B. Mahapatra and F. Weinberg: *Metall. Trans. B*, **18** (1987), 425.
18) I. Ziv and F. Weinberg: *Metall. Trans. B*, **20** (1989), 731.
19) J. W. Fernihough, S. L. Cockcroft, A. Mitchell and A. J. Schmalz: Superalloys 1996, Eds by R. D. Kissinger, D. J. Deye, D. L. Anton, A. D. Cetel, M. V. Nathal, T. M. Pollock and D. A. Woodford, TMS, Warrendale, PA, (1996), 481.
20) M. Bobadilla, J. Lacaze and G. Lesoult: *J. Cryst. Growth*, **89** (1988), 531.
21) J. W. Fernihough: Ph. D. Thesis, The University of British Columbia, Vancouver, Canada, (1995).
22) Ch.-A. Gandin: From Constrained to Unconstrained Growth during Directional Solidification, *Acta Mater.*, **48** (2000), 2483.
23) P. Rousset, M. Rappaz and B. Hannart: *Metall. Mater. Trans. A*, **26** (1995), 2349.
24) J. Ampuero and M. Rappaz: 2nd report of the CERS #1718.1 project, Ecole Polytechnique Fédérale de Lausanne, Switzerland, (1990).
25) A. F. Giamei and B. H. Kear: *Metall. Trans.*, **1** (1970), 2185.
26) S. M. Copley, A. F. Giamei, A.F. Johnson and M. F. Hornbecker: *Metall. Trans.*, **1** (1970), 2193.
27) T. M. Pollock and W. H. Murphy: *Metall. Mater. Trans. A*, **27** (1996), 1081.
28) T. Magnusson: private communication, Norwegian University of Science and Technology, Trondheim, Norway, (1999).
29) R. D. Pehlke, A. Jeyrajan and H. Wada: Summary of Thermal Properties for Casting Alloys and Mold Materials, University of Michigan, (1982).
30) R. T. Southin: *Trans. Metall. Soc. AIME*, **239** (1967), 220.
31) A. Ohno: Solidification. The Separation Theory and its Practical Applications, Springer-Verlag, Berlin, Heidelberg, (1987).
32) W. C. Winegard and B. Chalmers: *Trans. Am. Soc. Met.*, **46** (1954), 1214.
33) W. W. Mullins and R. F. Sekerka: *J. Appl. Phys.*, **35** (1964), 444.
34) J. A. Spittle and M. R. Tadayon: *Cast Met.*, **7** (1994), 123.